JOURNAL OF THERMOPHYSICS AND HEAT TRANSFER
Vol. 10, No. 1, January–March 1996

Axisymmetric Analysis of Transient Thermoelastic Behaviors in Composite Brake Disks

Hyeon-Wu Sonn,* Chun-Gon Kim,† and Chang-Sun Hong‡
Korea Advanced Institute of Science and Technology, Taejon 305-701, Republic of Korea
and
Byung-Il Yoon§
Agency for Defense Development, Taejon 305-600, Republic of Korea

This article presents the transient thermoelastic behaviors of carbon/carbon composite brake disks in the brake housing during braking action. The heat transfer problem from frictional heat and the elastic problem dealing with thermomechanical deformation in brake contact are coupled to each other. The coupled heat and elastic analysis were carried out using the finite element method. The fully implicit transient scheme for the thermoelastic analysis was newly implemented to improve the accuracy of calculations at every time step. Since the heat capacity of carbon/carbon composite is very large, the high temperature of the brake disk system is confined to only the narrow regions near the friction surfaces. Therefore, the thermoelastic behaviors of carbon/carbon composite brake disk system were little affected by the thermal boundary conditions in the brake housing during braking action.

Nomenclature

$[C_T]$ = capacity matrix
c = specific heat
E = elastic modulus
h = convective heat transfer coefficient
$[K_T]$ = conductivity matrix
k = thermal conductivity
N = shape function
P = normal pressure on friction surfaces
P_h = hydraulic pressure
Q = heat source
q = heat flux
$\{R\}$ = resultant thermal loading in heat equation
r, θ, z = cylindrical coordinates
T = temperature
$\dot{T}$ = time rate of temperature
ρ = density

Subscripts
A = area
M = master nodes
n = normal direction
S = slave nodes
V = volume

Introduction

AIRCRAFT brake systems are usually composed of multiple disks, in which the wheel-driven rotors are sandwiched between stators held stationary by the brake structure. Braking action is achieved by pressing the disks with the use of hydraulic pressure, and heat is generated on the contacted surfaces of disks. Carbon/carbon composite brake disks provide adequate structural, thermal, and friction characteristics. For a normal landing, brake temperatures of 500°C are typical while temperatures up to 1300°C can be experienced during the short engagement time for an aborted takeoff. Also, the use of carbon/carbon brake disks offered a 60% weight savings compared with steel.[1] The transient thermoelastic behaviors of carbon/carbon composite brake disks in the brake housing should be analyzed to understand thermoelastic behaviors that are subjected to considerable thermal loading during braking action for designing the brake system of an aircraft.

The analysis of temperatures and stresses in the friction disks was performed for a steel multidisk system.[2] An assumption was made there that the distribution of normal pressures on friction surfaces does not depend on the thermal state of the disks and it is uniform. The calculation under this assumption underestimated the thermal stresses in the disks. The thermoelastic analysis of a steel multidisk brake was performed without the assumption of the uniform distribution of normal pressures on friction surfaces to overcome this disadvantage.[3] The finite difference method was used to solve the unsteady heat conduction problem while the finite element method (FEM) was used to solve the elastic problem. However, the nodes of the finite difference method were not coincident with those of the FEM.[2,3]

This article presents the transient thermoelastic behaviors of carbon/carbon composite brake disks in the brake housing during braking action. A finite element code was developed that allows an effective investigation of transient thermoelastic analysis. The finite element code used for obtaining the results in the present study has been verified by Sonn et al.[4] However, the present results were not verified experimentally because no experimental results were available for comparison.

The thermoelastic analysis of brake disks is represented as the coupled heat and elastic problems including nonisothermal and multipoint contact. The heat transfer problem from frictional heat and the elastic problem dealing with thermomechanical deformation in brake contact are coupled to each other. Therefore, the coupled heat equation and elastic equation with the contact conditions should be solved simultaneously. In this coupled thermoelastic analysis, the use of the

Received April 4, 1995; revision received Sept. 5, 1995; accepted for publication Sept. 14, 1995.

*Research Assistant, Department of Aerospace Engineering, 373-1 Kusong-dong, Yusung-gu.
†Associate Professor, Department of Aerospace Engineering, 373-1 Kusong-dong, Yusung-gu. Member AIAA.
‡Professor, Department of Aerospace Engineering, 373-1 Kusong-dong, Yusung-gu. Member AIAA.
§Principal Researcher, Advanced Technology Research Center 3-4, P.O. Box 35, Yusung-gu.

FEM for heat transfer analysis is preferable because node point temperatures are needed for thermal stress analysis. Therefore, in this study, the coupled heat and elastic analysis was carried out using the FEM different from other previous researches.[2,3] In addition, the fully implicit transient scheme for the thermoelastic analysis was newly implemented to improve the accuracy of calculations at every time step. The advantage of using this finite element code is that the efficiency of the calculation is increased because the same node point variables of the same mesh layout are used in both heat and elastic analysis. The present work is based on the fully coupled theory that stresses and temperature fields are mutually influenced. Temperature fields and deformations are assumed axisymmetric. The wear in a short engagement time is so small that it is neglected in this analysis.

Governing Equations

In thermally orthotropic materials, the transient heat conduction equation can be written as follows[5]:

$$(k_{lm}T_{,m})_{,l} + Q = \rho c\dot{T} \qquad (l, m = 1, 2, 3) \tag{1}$$

Equation (1) is solved with the prescribed temperature (Dirichlet condition), the prescribed convection (Cauchy condition), and the prescribed heat flux (Neumann condition) boundary conditions and the initial condition.

Using the Galerkin's method, the finite element formulation of unsteady heat, Eq. (1), is performed as follows:

$$\int_V N_i \rho c N_j \, dV\dot{T}_j + \int_V N_{i,l} k_{lm} N_{j,m} \, dV T_j + \oint_{A1} N_i h N_j \, dA T_j = \int_V N_i N_j \, dV Q_j + \oint_{A1} N_i h T_\infty \, dA - \oint_{A2} N_i q_n^* \, dA \qquad (i, j = 1, 2, \ldots, 8) \tag{2}$$

Equation (2) can be written in matrix form as

$$[C_T]\{\dot{T}\} + ([K_T] + [H_T])\{T\} = \{R_Q\} + \{R_\infty\} - \{R_{q_n}\} \tag{3}$$

Heat Eq. (3) has the following form:

$$[C_T]\{\dot{T}\} + [K_H]\{T\} = \{R\} \tag{4}$$

where $[K_H] = [K_T] + [H_T]$, $\{R\} = \{R_Q\} + \{R_\infty\} - \{R_{q_n}\}$.

In the present work, the direct integration method was selected that is a useful solution method for transient problems. A direct integration scheme is based on the following relation:

$$\{T\}_{t+\Delta t} = \{T\}_t + [(1 - \beta)\{\dot{T}\}_t + \beta\{\dot{T}\}_{t+\Delta t}]\Delta t \tag{5}$$

An implicit method is developed from Eqs. (4) and (5) as

$$([C_T] + \beta\Delta t[K_H])\{T\}_{t+\Delta t} = ([C_T] - (1 - \beta)\Delta t[K_H])\{T\}_t + (1 - \beta)\Delta t\{R\}_t + \beta\Delta t\{R\}_{t+\Delta t} \tag{6}$$

From a known initial temperature $\{T\}_0$, the history of temperature is generated by Eq. (6). Equation (6) contains a factor β that the analyst may select.[6] In this analysis, $\beta = 0.8$ was used, which is an unconditionally stable scheme.

The elastic equation of static equilibrium may be derived by using Galerkin's method similar to the previous heat equation as[7]

$$[K]\{U\} = \{F_f\} + \{F_p\} + \{F_T\} \tag{7}$$

Model of Multiple Brake Disks

Configuration of Brake Disks

In this work, the r, θ, and z cylindrical coordinates are used. Figure 1 shows the configuration of a rotor and a stator for an aircraft brake system and the contact surface between a stator and a rotor on which heat is generated in the r-θ plane. The rotors are driven by the wheel and the stators are held stationary by the brake structure. By pressing the disks with hydraulic pressure, disks contact each other, and so heat is generated on the contacted friction surfaces. The shape of the contacted surfaces is annular, and hence, it is assumed that temperature fields and deformations are axisymmetric with respect to the z axis.

The schematic cross section of an aircraft brake system in the r-z plane is shown in Fig. 2. Only one-half of the cross section is shown because it is an axisymmetric model with respect to the z axis. The friction surfaces are numbered 1–6 from the right-hand side (RHS) of the brake disk system.

Contact Problem of Multiple Brake Disks

The present model is a special case of the contact problem because it is nonisothermal and contact points appear simultaneously on many surfaces. In contact problems, the contact interfaces do not have prescribed displacements or tractions. Instead, they must satisfy two relationships such as the continuity of displacements in the normal contact direction (that means no overlap of contact area) and the equilibrium conditions (equal and opposite tractions). Although each contacting body may be assumed to be linear material, contact problems are nonlinear because the contact area does not change linearly with the applied load. Therefore, any computer program for contact problem must include some forms of iterations. The iterations to obtain the actual contact areas are terminated when all of these conditions are met.[8]

Let the interface of the two disks under consideration be a friction surface. In each friction surface a pair of contacted nodes is defined. One of the nodes is designated as the master node and the other as the slave node. Then, continuity of the axial displacements at this interface is required for each pair of contact nodes, however, discontinuity of the radial displacements can take place due to the slip at the interface. The

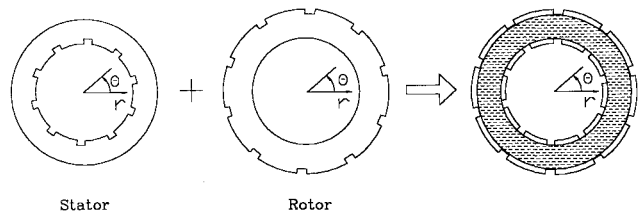

Fig. 1 Configuration of a stator and a rotor for an aircraft brake system (heat is generated on the annular hatched surface).

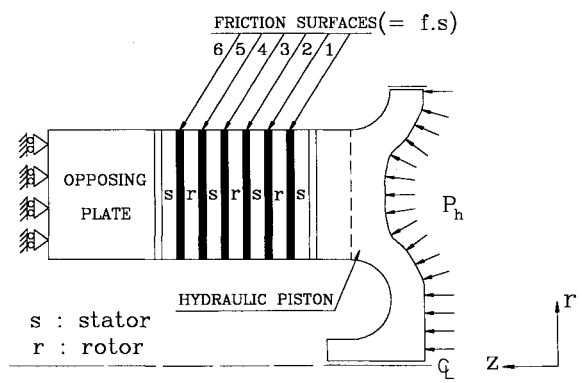

Fig. 2 Schematic cross section of an aircraft brake system.

following constraint conditions are needed for each pair of master and slave nodes at the interface:

$$u_{zatM} = u_{zatS} \quad \text{when } P > 0 \tag{8}$$

$$u_{zatM} \neq u_{zatS} \quad \text{otherwise} \tag{9}$$

On the friction surfaces, sliding in the circumferential direction takes place. The radial component of the sliding velocity resulting from the deformations of the disks is considerably smaller than the circumferential component. An analogous relation holds between corresponding components of the frictional forces. Thus, almost no frictional forces on the friction surfaces arise. In this sense the contact of the present model is frictionless in the radial direction.[9]

By the continuity condition of the temperature field, nodal temperatures on the friction surfaces have the following constraint condition:

$$T_M = T_S \quad \text{when } P > 0 \tag{10}$$

By the relation $q^* = \mu Pr\omega$, heat that is called as brake capacity is generated on the contacted nodes of the friction surfaces:

$$q^* = \mu Pr\omega \quad \text{when } P > 0 \tag{11}$$

$$q^* = 0 \quad \text{otherwise} \tag{12}$$

Finite Element Models with Elastic and Heat Boundary Conditions

Figure 3 shows the finite element model of carbon/carbon composite brake disks with elastic boundary conditions in the brake housing. The inner radius r_i, the outer radius r_o, and the thickness of a disk are 0.11, 0.16, and 0.015 m, respectively, in the present model. The A-B surface along the radius of the right-end disk at $z = 0.0$ m is pressed by the hydraulic pressure and the C-D surface along the radius of the left-end disk at $z = 0.105$ m rests on the opposing plate. On the friction surfaces, the constraint Eqs. (8) and (9) are to be applied. Axisymmetric 8-node isoparametric elements were used for the finite element analysis of the brake disk system, where there are 85 elements and 300 nodes per disk. The model contains 7 brake disks, and the whole system has 595 elements and 2100 nodes. The adequate number of elements used in the present transient analysis is very important because of the calculation time. As the change of stress or heat flux gradients is remarkable at the boundaries of a disk, the mesh-refinement is required. By using the mapping function of $f(x) = x - 0.2 \sin(2\pi x)/2\pi$, the finer mesh near the boundaries of a disk was adopted.

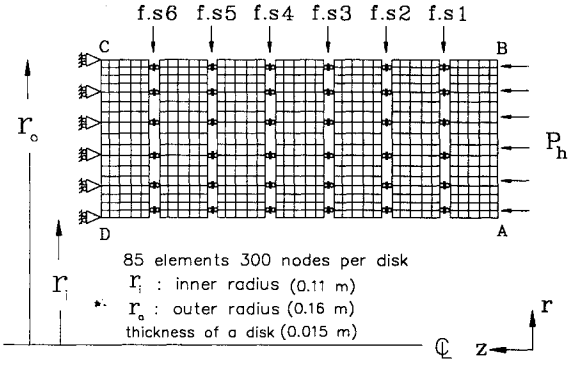

Fig. 3 Axisymmetric elastic finite element model for the thermoelastic analysis.

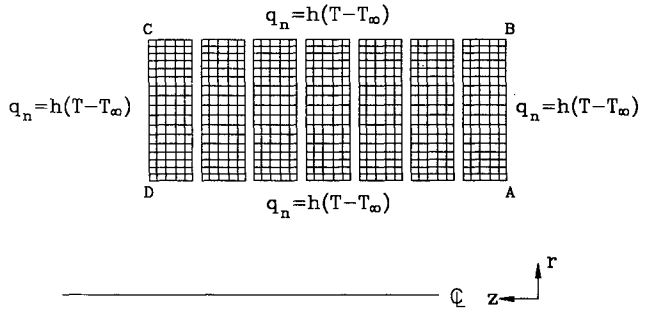

Fig. 4 Axisymmetric heat finite element model for the thermoelastic analysis.

Figure 4 shows the same finite element model with convective heat transfer boundary conditions. On the friction surfaces, constraint Eqs. (10–12) were applied. Three types of thermoelastic model were studied to investigate the effect of boundary conditions on the interior thermoelastic behaviors of brake disks.

The thermoelastic model having the convective heat transfer boundary condition on all boundaries was designated as model-A. Model-A has the prescribed convective boundary conditions (Cauchy condition), $q_n = h(T - T_\infty)$. If h is zero, then the model has an adiabatic boundary condition (Neumann condition), $q_n = 0$. The thermoelastic model that has the adiabatic boundary conditions on all A-B, B-C, C-D, and D-A boundaries was designated as model-B. The thermoelastic model that has the Dirichlet conditions was designated as model-C. The boundary conditions for this model-C are as follows: the adiabatic condition is applied to the two surfaces bound by r_o and r_i, and the temperature on the A-B and C-D surfaces has a prescribed temperature boundary condition (Dirichlet condition), $T = 20°C$ by the assumption of the cooling state (e.g., air blowing).

Method of Solving the Coupled Thermoelastic Problem

In this coupled thermoelastic analysis, heat Eq. (6) concerning frictional heat, and elastic Eq. (7) dealing with thermomechanical deformation, are coupled to each other. There-

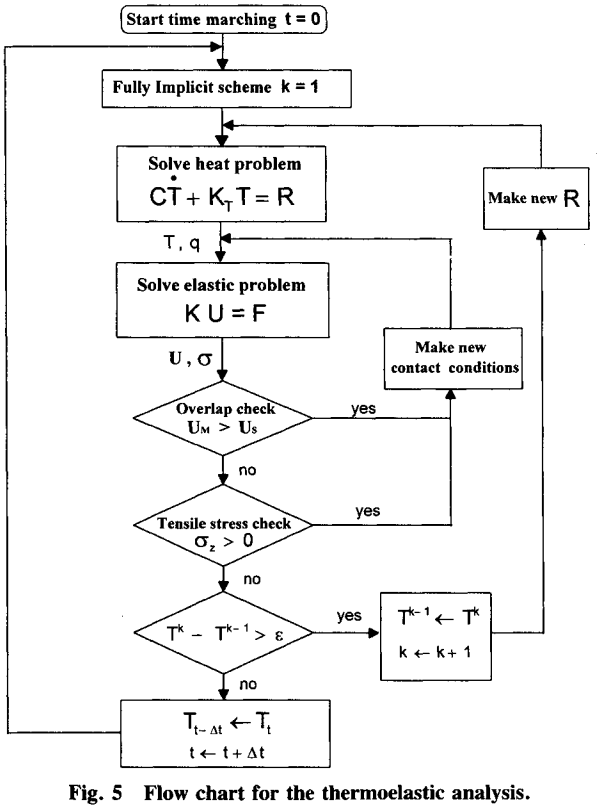

Fig. 5 Flow chart for the thermoelastic analysis.

fore, Eqs. (6) and (7) should be solved simultaneously. When solving the problem of transient heat conduction the solutions are computed with the time step Δt. If t is the time at which the solution is known, the solution for the next time step $t + \Delta t$ needs the computation of the RHS of Eq. (6), $\{R\}_{t+\Delta t}$. However, the distributions of P on the friction surfaces at this time step, appearing in the thermal boundary conditions of Eq. (11), are not known. For this reason, Ref. 3 approximated $P(t)$ with the total force represented by the applied hydraulic pressure $P_h(t)$ of known time function, as shown next:

$$P(t + \beta\Delta t) \approx P(t) \frac{P_h(t + \beta\Delta t)}{P_h(t)} \tag{13}$$

As the contact areas on friction surfaces are changing with time in this thermoelastic analysis for brake disks, the assumption of Eq. (13) may be unreasonable. Therefore, in the present work, the fully implicit transient scheme was implemented without the unreasonable assumption such as Eq. (13) to compute the RHS of Eq. (6), $\{R\}_{t+\Delta t}$, accurately.

Figure 5 shows the flow chart for the transient thermoelastic analysis. In the time loop, the superscript k means the number of iteration steps. At time t, solving Eq. (6) yields the temperature distribution $\{T\}^k$. Using this $\{T\}^k$, the load vector due to thermal expansion $\{F_T\}^k$ in Eq. (7) can be obtained. To solve the contact problem, Eq. (7) is solved by an iteration method. That is, new contact conditions and new stresses are computed from Eq. (7) iteratively to meet the no-overlap condition and the equilibrium condition on the contact area. The fully implicit transient iterations are repeated at every time step to obtain the equilibrium solution of the coupled thermoelastic equations until $\{T\}^k$ and $\{T\}^{k-1}$ are nearly the same. During the process, new resultant thermal loading $\{R\}_t^k$ in Eq. (6) can be constructed by the relation of brake capacity Eq. (11). From $\{R\}_t^k$ and new equilibrium contact condition at t, the heat Eq. (6) at $t + \Delta t$ can be solved by carrying out the time marching. In this way, the history of thermoelastic state at any time could be generated.

Results

The properties of carbon/carbon for the calculation of the thermoelastic analysis are shown in Table 1. Carbon/carbon composite brake disk is usually fabricated to show a transversely isotropic behavior in the r-θ plane to provide adequate structural, thermal, and friction characteristics at the same time. However, the material properties in the r-z plane are inevitably orthotropic due to the laminated nature of the carbon/carbon brake disk. Therefore, many material properties for heat analysis as well as elastic analysis are needed in the thermoelastic analysis of carbon/carbon composite brake disks.

Table 1 Properties of carbon/carbon for the calculation of the thermoelastic analysis

Properties	Symbol	Value
Elastic modulus in r direction	E_r	50.2 GPa
Elastic modulus in z direction	E_z	5.89 GPa
Shear modulus in r-z plane	G_{rz}	2.46 GPa
Poisson's ratio in r-θ plane	$\nu_{r\theta}$	0.3
Poisson's ratio in r-z plane	ν_{rz}	0.33
Thermal expansion coefficient in r direction	α_r	0.31×10^{-6}/K
Thermal expansion coefficient in z direction	α_z	0.29×10^{-6}/K
Thermal conductivity in r direction	k_r	50 W/(m K)
Thermal conductivity in z direction	k_z	10 W/(m K)
Density	ρ	1.8×10^3 kg/m^3
Specific heat	c	1.42×10^3 J/(kg K)
Convection coefficient	h	454.5 W/(m^2 K)
Friction coefficient	μ	0.3

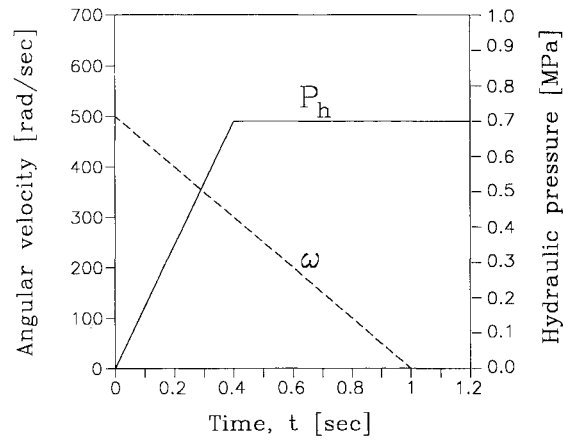

Fig. 6 Time history of the angular velocity and the hydraulic pressure.

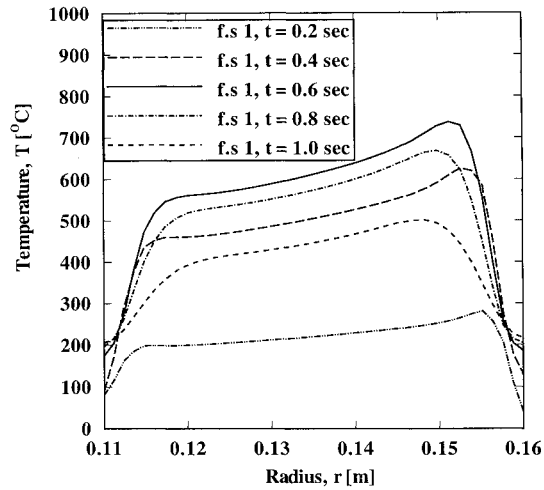

Fig. 7 Temperature distributions along the friction surface 1 for t = 0.2–1.0 s.

Figure 6 shows the time history of $P_h(t)$ and $\omega(t)$ adopted for the present modeling analysis. The applied hydraulic pressure $P_h(t)$ was assumed to linearly grow up to 0.7 MPa by 0.4 s, and then kept constant. The angular velocity $\omega(t)$ was assumed to linearly decay and finally become zero in 1.0 s. The implicit transient time step Δt = 0.0001 s was used in the calculations.

Thermoelastic Behaviors of Model-A

Figure 7 shows the typical temperature distributions on friction surface 1 with the lapse of time. The temperature distributions on friction surfaces 1–6 had nearly the same trend for the boundary condition of model-A. At t = 0.6 s, the temperature distribution shows the maximum value during the entire application time span.

To obtain a clear view of the thermoelastic behaviors of the present brake disk system, the transient responses of the thermal state are shown in Figs. 8a–8c for t = 0.2, 0.6, and 1.0 s, respectively. The temperature distributions show high gradients near the narrow regions of the friction surfaces. It was observed that the temperature of outer radius is a little higher than that of inner radius.

Figure 9 shows the maximum temperature history in the brake disk system. The maximum temperature in the system increases by t = 0.6 s and then decreases. Since there exists an overshoot of temperature during the thermoelastic process of the brake disk system, it is necessary to perform the transient thermoelastic analysis in the brake disk to understand

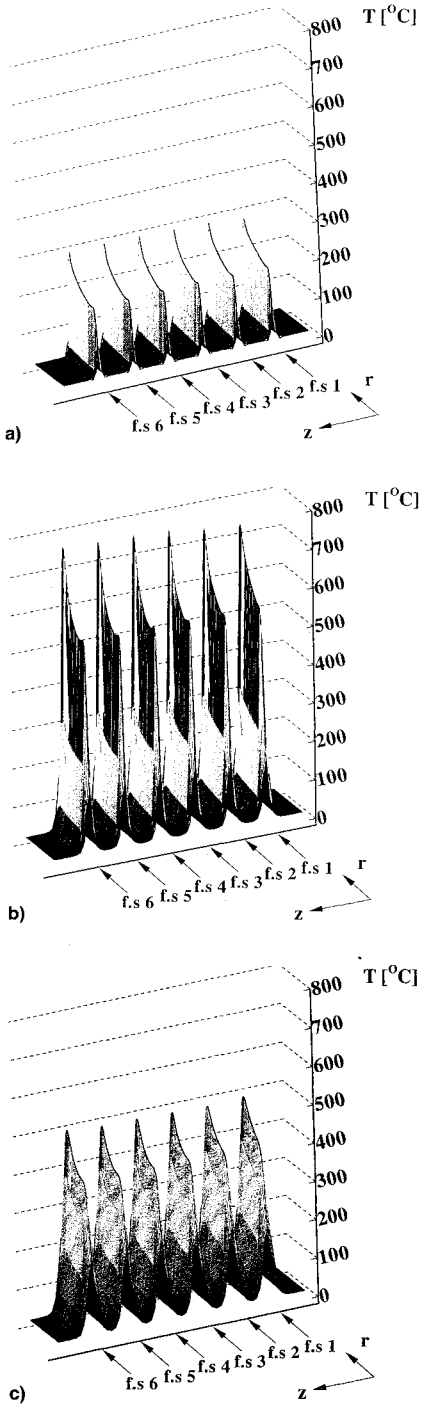

Fig. 8 Temperature distributions of the multidisk system: a) maximum T = 296°C at t = 0.2 s, b) maximum T = 764°C at t = 0.6 s, and c) maximum T = 507°C at t = 1.0 s.

its thermoelastic behaviors accurately. The overshoot of temperature stems from the used material properties and/or the inputs, $P_h(t)$ and $\omega(t)$.

Figure 10 shows the typical temperature fields of the carbon/carbon composite brake disk system at t = 0.6 s. Since the heat capacity ρc of carbon/carbon composite is very large, the thermal diffusivity is very small. Therefore, the high temperature of the brake disk system is confined only to the narrow regions near friction surfaces.

Figure 11 shows the typical pressure distributions along only friction surface 1 for t = 0.1–1.0 s, because the pressure distributions along friction surfaces 1–6 also have the same trend. The history of the pressures nearly matches that of the applied braking pressure $P_h(t)$ and no abrupt change of pressure distribution occurs along the friction surfaces. The present analysis for carbon/carbon composite brake disk system (orthotropic case) shows relatively uniform pressure distributions along the friction surfaces when compared with the results of the steel brake disk system (isotropic case) in Ref. 3.

Figure 12 shows the typical contact areas on the friction surfaces of the brake disk system at t = 0.6 s. The contact

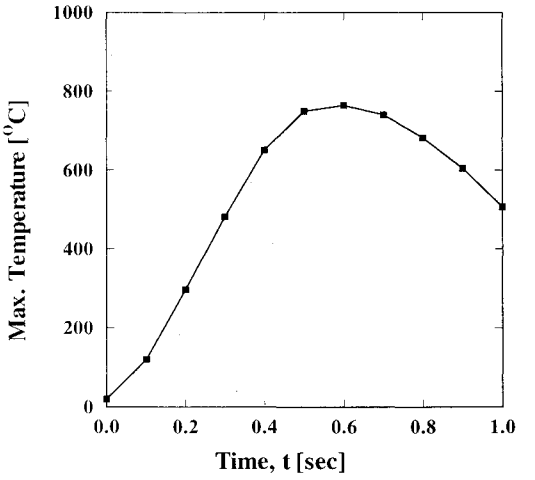

Fig. 9 Maximum temperature history in the brake system.

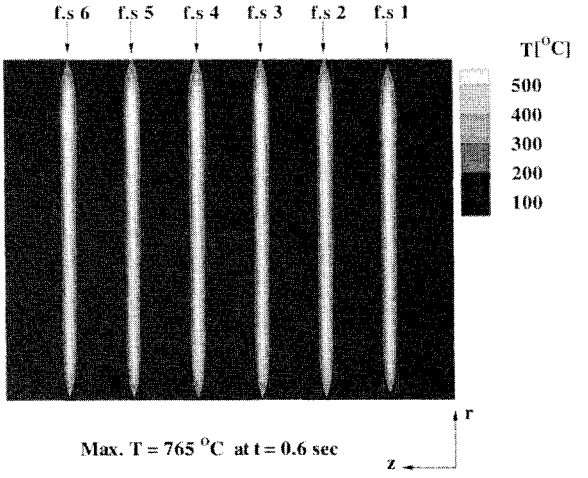

Fig. 10 Temperature fields of the brake system at t = 0.6 s.

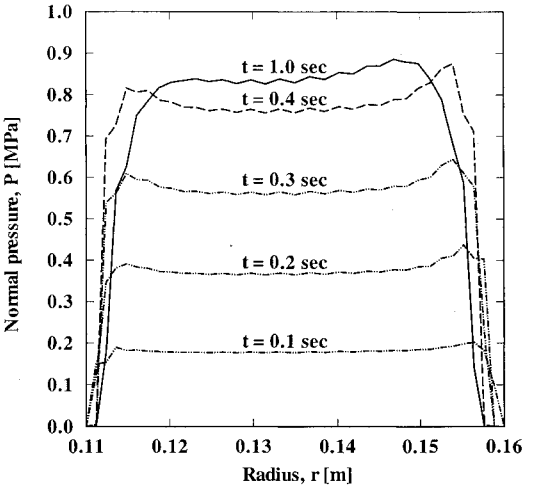

Fig. 11 Pressure distributions along the friction surface 1 for t = 0.1–1.0 s.

areas of the present carbon/carbon composite brake disk system (orthotropic case) are very uniform and large when compared with the results of the steel brake disk system (isotropic case) of Ref. 3. The reason is that the contact area decreases as the stiffness in thickness direction E_z increases up to the isotropic case of $E_z = E_r$. Thus, the carbon/carbon composite brake disks show good performance as a brake friction material because of the large contact area and the overall uniform pressure distributions along the friction surfaces in addition to the large heat capacity ρc.

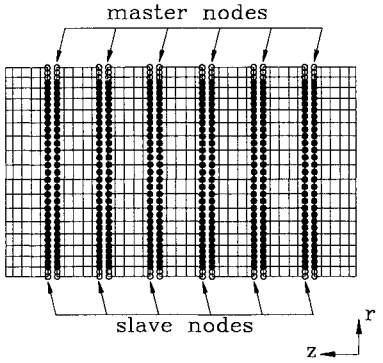

Fig. 12 Contact areas on the friction surfaces at $t = 0.6$ s, ○ = detached master and slave node; ● = contacted master and slave node.

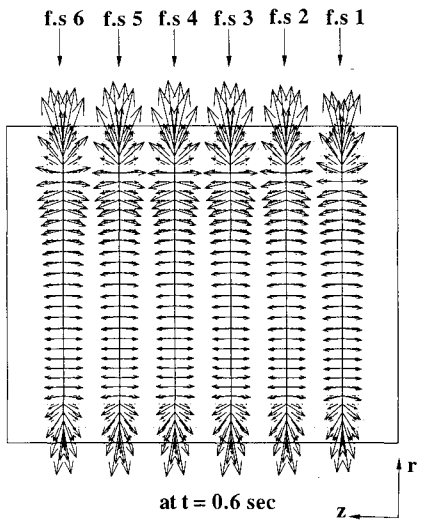

Fig. 13 Heat flux vectors in the brake system at $t = 0.6$ s.

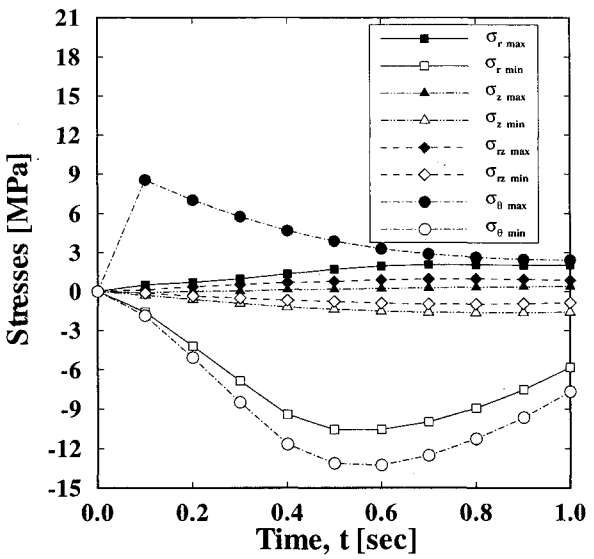

Fig. 14 Variation of stress components with the change of time.

Figure 13 represents the typical heat flux vectors of the brake disk system at $t = 0.6$ s. Heat flux vectors are large in only the narrow regions near friction surfaces because heat generation on friction surfaces is very large in spite of heat convection on boundaries. Heat flux is concentrated at the local regions of existing the geometric singularity as heat flows through only the contacted area. The larger the contact areas on friction surfaces, the smoother the heat of the brake disk system flows.

Figure 14 shows the stress components of the brake disk system with the change of time. Solid symbols mean the upper-bound of stress components and hollow symbols are the lower-bound of stress components. In an axisymmetric model, there are four stress components σ_r, σ_θ, σ_z, and σ_{rz}. At the initial time $t = 0.1$ s, σ_θ has the highest tensile stress value and σ_r has the highest compressive stress value. At $t = 0.6$ s, σ_θ shows the highest compressive stress value. In the viewpoints of the maximum stress failure, σ_θ and σ_r are likely to be considered as the dominant components. However, σ_z and σ_{rz} are likely to be considered as the minor stress components in this thermoelastic analysis.

Effect of Three Types of Boundary Conditions

Thermoelastic model-B and model-C were also studied to investigate the effect of thermal boundary conditions on the interior thermoelastic behaviors of brake disks. In addition, the case of a large $h = 4545$ W/(m^2 K) of model-A was also investigated. Surprisingly, the thermoelastic behaviors of all of the models were almost the same as the previous results of model-A. This shows that carbon/carbon composite brake disks act as a heat sink for such a short engagement time. Therefore, the proportion of heat dissipated into the atmosphere in this period is negligible. For example, the temperatures of the A-B surface along the radius of the right-end disk at $z = 0.0$ m were nearly kept to room temperature, 20°C independent of thermoelastic model-A, model-B, and model-C when $c = 1420$ J/(kg K). To verify this conclusion, the case of small specific heat $c = 142$ J/(kg K) of model-A was studied.

Figure 15 shows the temperatures of the A-B surface along the radius for thermoelastic model-A, model-B, and model-C when $c = 142$ J/(kg K). The temperatures of the A-B surface are clearly dependent on the three types of thermoelastic model-A, model-B, and model-C for the case of $c = 142$ J/(kg K). Therefore, it is concluded that the effect of thermal boundary conditions on the interior thermoelastic behaviors of brake disks becomes important only for the case of small heat capacity.

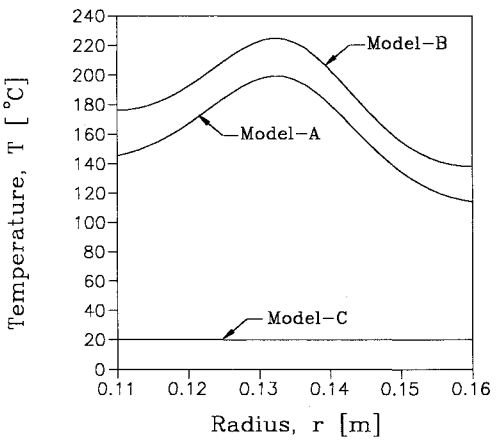

Fig. 15 Temperature distributions along the A-B surface of all the models when $c = 142$ J/(kg K) at $t = 1.0$ s.

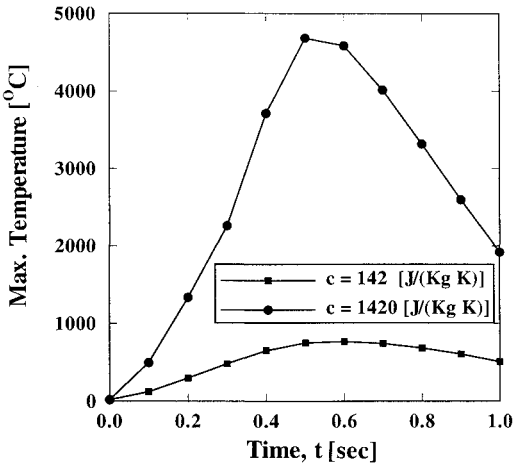

Fig. 16 Maximum temperature history in the brake system with variations of specific heat.

Figure 16 shows the maximum temperature history for the interior of the brake disk system of model-A when $c = 142$ and 1420 J/(kg K), respectively. The maximum temperature for $c = 142$ J/(kg K) is nearly six times higher than that of $c = 1420$ J/(kg K) at $t = 0.6$ s. That is, the value of ρc is the main factor that influences the effect of the thermal boundary conditions as well as the thermoelastic state in a brake disk system.

It can be concluded that a carbon/carbon composite brake disk system has little dependency on the thermal boundary conditions of the system, especially the convective heat transfer coefficient because of the large ρc.

Conclusions

A finite element code was developed that is adequate for the transient thermoelastic analysis of carbon/carbon composite brake disks for an aircraft. When compared with the previous researches, the efficiency of calculation was improved by using the same mesh layout in the heat and the elastic analysis. Also, the fully implicit transient scheme for the thermoelastic analysis was newly implemented to improve the accuracy of calculations at every time step.

Because the heat capacity of carbon/carbon composite is very large, thermal diffusion is very slow. Therefore, the high temperature of the brake disk system is confined only to the narrow regions near the friction surfaces. Parametric studies on the brake disk system were conducted for various thermal boundary conditions and convective heat transfer coefficients. For the usual heat capacity range of carbon/carbon composite materials, the internal thermoelastic states of the present brake system were almost unaffected by the various thermal boundary conditions as well as the convective heat transfer coefficients. It is therefore concluded that the thermoelastic behaviors of the carbon/carbon composite brake disk system are little affected by the thermal boundary conditions and convective heat transfer coefficient in the brake housing during braking action because of the small thermal diffusivity. Since the carbon/carbon composite brake disk system shows uniform and mild pressure distributions along the friction surfaces, it can provide good braking performance. In addition, it is observed that the circumferential stress component σ_θ and the centrifugal stress component σ_r in the brake disk system are the dominant stress components from the viewpoint of the maximum stress failure criterion.

References

[1]Stimson, I. L., and Fisher, R., "Design and Engineering of Carbon Brakes," *Philosophical Transactions of the Royal Society of London, Series A: Mathematical and Physical Sciences*, Vol. 294, No. 1411, 1980, pp. 175–182.

[2]Zagrodzki, P., "Numerical Analysis of Temperature Fields and Thermal Stresses in the Friction Discs of a Multidisc Wet Clutch," *Wear*, Vol. 101, No. 3, 1985, pp. 255–271.

[3]Zagrodzki, P., "Analysis of Thermomechanical Phenomena in Multidisc Clutches and Brakes," *Wear*, Vol. 140, No. 2, 1990, pp. 291–308.

[4]Sonn, H. W., Kim, C. G., Hong, C. S., and Yoon, B. I., "Transient Thermoelastic Analysis of Carbon/Carbon Composite Brake Disks," *Journal of Reinforced Plastics and Composites* (to be published).

[5]Hetnarski, R. B., "Basic Equations of the Theory of Thermal Stresses," *Thermal Stresses I*, edited by R. B. Hetnarski, Elsevier, Amsterdam, 1986, pp. 2–20.

[6]Reddy, J. N., *An Introduction to the Finite Element Method*, McGraw–Hill, New York, 1984, pp. 50–52.

[7]Burnett, D. S., *Finite Element Analysis*, Addison–Wesley, Reading, MA, 1987, pp. 730–777.

[8]Becker, A. A., *The Boundary Element Method in Engineering*, McGraw–Hill, New York, 1992, pp. 161–171.

[9]Mahmoud, F. F., Salamon, N. J., and Marks, W. R., "A Direct Automated Procedure for Frictionless Contact Problems," *International Journal for Numerical Methods in Engineering*, Vol. 18, No. 2, 1982, pp. 245–257.